Mechanistic Insights into the Activity of Mo-Carbide Clusters for Methane Dehydrogenation and Carbon-Carbon Coupling Reactions to Form Ethylene in Methane Dehydroaromatization

Article *in* The Journal of Physical Chemistry C · May 2018

DOI: 10.1021/acs.jpcc.7b09275

CITATION
1

READS
81

5 authors, including:

Tuhin Suvra Khan
Indian Institute of Technology Delhi
28 PUBLICATIONS **301** CITATIONS
SEE PROFILE

Sonit Balyan
Indian Institute of Technology Delhi
2 PUBLICATIONS **2** CITATIONS
SEE PROFILE

Ali Haider
Indian Institute of Technology Delhi
57 PUBLICATIONS **328** CITATIONS
SEE PROFILE

THE JOURNAL OF PHYSICAL CHEMISTRY C

Subscriber access provided by INDIAN INST OF TECH NEW DELHI

C: Surfaces, Interfaces, Porous Materials, and Catalysis

Mechanistic Insights into the Activity of Mo-Carbide Clusters for Methane Dehydrogenation and Carbon-Carbon Coupling Reactions to Form Ethylene in Methane Dehydroaromatization

Tuhin Suvra Khan, Sonit Balyan, Sourabh Mishra, Kamal K. Pant, and M. Ali Haider

J. Phys. Chem. C, **Just Accepted Manuscript** • DOI: 10.1021/acs.jpcc.7b09275 • Publication Date (Web): 11 May 2018

Mechanistic Insights into the Activity of Mo-Carbide Clusters for Methane Dehydrogenation and Carbon-Carbon Coupling Reactions to Form Ethylene in Methane Dehydroaromatization

Tuhin Suvra Khan[a,$,*], Sonit Balyan[a,*], Sourabh Mishra[a,*], Kamal K. Pant[a,$] and M. Ali Haider[a,$]

[a] Department of Chemical Engineering, Indian Institute of Technology Delhi, Hauz Khas, New Delhi-110016, India

[$]Corresponding authors E-mail: tuhinsk@iitd.ac.in, kkpant@chemical.iitd.ac.in, haider@iitd.ac.in

*equal first author contribution

Abstract

Methane dehydrogenation and C-C coupling reactions to form ethylene on two different carbide clusters of molybdenum (Mo_4C_2 and Mo_2C_6) were studied. Density functional theory (DFT) calculations were performed to understand the reactivity of the two clusters, linking it to the overall methane dehydroaromatization (MDA) process. The electronic effect of catalyst reduction procedures and anchoring of the cluster on the zeolite framework was captured in simulations with varying positive charge on the cluster. In general, with one exception, DFT calculations suggested a reduction in dehydrogenation activation energies with more reduced (lesser positive charge) clusters. Similarly, activation barriers for the transfer of a H atom from the carbon to neighboring Mo site were calculated to be lower on more reduced clusters. In contrast, the coupling reactions of the two CH_3 and the two H atoms on the surface showed a reverse trend. The activation energies of the C-C and the H-H coupling steps were observed to be lower on less reduced (higher positive charge) clusters. On comparing the two (Mo_4C_2 and Mo_2C_6) clusters with similar charges, the activation energies for the first methane dehydrogenation were observed to be of similar value on both clusters for the neutral charge. However, second methane dehydrogenation was calculated to show a significantly higher barrier on the Mo_2C_6 cluster for both neutral and +1 charge. In addition, CH_3 coupling reaction was facilitated with relatively lower activation barrier on the Mo_2C_6 cluster, as compared to the Mo_4C_2 cluster. Thus, Mo_2C_6 sites in the vicinity of the Brønsted acid sites of the zeolite, are likely to be more active for the coupling of the two CH_3 species and helpful in MDA. This

alluded to the operando experimental findings by Lezcano-González *et al.* [*Angew. Chem., Int. Ed.* **2016**, *55*, 5215–5219], wherein it was suggested that methane might be activated on carbide and oxycarbide species, however; formation of MoC_3 type species on stream was linked directly to MDA.

Keywords: methane dehydroaromatization, carbide cluster, zeolite, dehydrogenation and heterogeneous catalyst

Introduction

Recent discovery of shale gas reserves as a cheap and abundant energy source has necessitated efforts in research for its conversion into higher value and transportable products [1–6]. Since natural gas comprises primarily of methane, a non-oxidative process to directly convert methane into aromatics is receiving due attention. Possibly, due to its safe nature (as compared to explosive combustion in presence of oxygen)[7], easy transportability (as compared to direct natural gas transportation)[4,8,9] and ability to operate at on-site remote locations (without any reagent)[7]. However, thermodynamics dictates the unfavorable nature of direct MDA to benzene[1,4,5] and only at high temperatures (>700 °C) the reaction yields benzene with high selectivity (~80%) and appreciable conversion (10%)[5,10]. Moreover, the propensity to form coke is higher as compared to aromatics, leading to rapid catalyst deactivation with sintering and pore blockages by the condensation of polynuclear aromatic hydrocarbons[6,11–13]. Widely used catalyst for MDA consists of molybdenum supported on a zeolite (Mo/HZSM-5 or Mo/HMCM-22)[1,5]. Catalyst in general is suggested to be bi-functional, wherein dehydrogenation and first C-C coupling to form ethylene occur on the active Mo sites and the Brønsted acid sites of the zeolite are responsible for chain growth and aromatization[1,2,14]. Active site for methane activation on Mo is rigorously debated and is thought to be an oxide[15], oxycarbide[7,16–18] or carbide[7,14,17,19]. During the initial induction period, the oxide MoO_x species are carburized to form an oxycarbide and later a carbide. Recent experimental investigations under operando conditions lead by Beale, Weckhuysen and co-workers had attributed methane activation at the start of the reaction to the oxycarbide (MoC_xO_y) species[17]. However, benzene formation was only achieved when MoO_x was completely carburized to form MoC_3 species, suggesting synergistic interaction between MoC_3 with the neighboring Brønsted sites in aromatization[17]. The MoC_3 on prolong operations

was further suggested to migrate and sinter to form Mo_2C type large nanoparticles leading to a reduction in the number and accessibility of the active sites[17]. Interestingly, previous experimental studies by Ichikawa and co-workers using XANES/EXAFS had identified Mo_2C cluster as the sites for methane activation[20].

Predicting the correct structure of carbide species formed during its continuous evolution on stream and correlating its activity to MDA is a difficult task. Discrepancies may partially arise from the fact that the activity of the carbide species formed is indirectly dictated by the anchoring of the precursor oxide species on the zeolite framework. It was demonstrated in a separate study by Podkolzin, Wachs, and co-workers, utilizing a combination of spectroscopic experiments and theory[7]. On calcination at 773 K, Mo existed in +6 oxidation state, forming a charged dioxo $Mo(=O)_2^{2+}$ species anchored on the two oxygen atoms, which was coordinated with two separate Al atoms of the zeolite framework. On increasing the Si/Al ratio, the same species may be anchored on a single Al atom site as $Mo(=O)_2(OH)^+$. In a dealuminated zeolite, or on the prolonged regeneration of the catalyst in the presence of oxygen, the dioxo species were observed to migrate and anchor on Si sites of the external zeolite surface. The most stable Mo carbide nanostructure, Mo_4C_2, formed at the reaction temperature (>973 K) was calculated to activate methane with a reduced activation barrier (E_a=112 kJ/mol)[7] when anchored to the dual Al sites of the zeolite framework as compared to when anchored on the external Si sites (E_a=140 kJ/mol). A search for other stable carbide clusters by the same group using genetic algorithms and DFT calculations had predicted the structure of Mo_2C_6 to be equally stable and important[19].

Developing an understanding on the activity of both carbide clusters (Mo_4C_2 and Mo_2C_6) is necessary, since similar species were suggested to form in the operando experiments[7,17] and were ascribed as the active sites. Depending on the anchoring site and corresponding reduced state (charge) of the cluster, the reactivity towards C-H bond activation and C-C coupling reactions is expected to vary. Therefore, to develop a comprehensive insight, a study on the effect of cluster charge on C-H activation and C-C coupling is necessary. The aforementioned studies have established the importance of controlling the nature of active sites in ensuring catalyst stability and achieving higher aromatic selectivity. The study presented here utilizes DFT calculation on the two clusters to draw a parallel between reaction energetics and cluster charge. The mechanistic view thus developed is expected to provide the key to engineer the active site by

utilizing a different dopant or may be a different support. In addition, a systematic protocol may be developed for treating the deactivated catalyst, to regain the active site in cyclic operations.

Computational Method

Non-periodic, all electron DFT calculations for both neutral and charged Mo_xC_y clusters were performed using double numerical plus polarization function (DNP) basis set as available in DMol^3 module of Material Studio 8 (Biovia, San Diego, USA)[21]. Non-local generalized gradient approximation (GGA) corrected by Perdew and Wang (PW91)[22] was utilized as the exchange-correlation functional. The GGA-PW91 is extensively used as the exchange-correlation functional in modeling catalytic systems comprising of transition metal carbides[23–28].

For obtaining self-consistent field (SCF) density convergence criteria of $1e^{-6}$ was applied and the maximum allowed change was specified by a mixing parameter of 0.2 and 0.5 for charge and spin density, respectively. In order to improve the SCF convergence, smearing of 0.005 a.u. was used. Convergence criteria for geometry optimization were set to 0.0001 eV, 0.05 eV/Å, and 0.005 Å with respect to energy, force, and atom displacement, respectively. DMol^3 utilizes a 3D numerical integration procedure to solve the integrals involved.

Structures of the transition state (TS) for reaction steps were calculated using the TS search available in DMol^3, which was performed with linear synchronous transit/quadratic synchronous transit (LST/QST) method[29]. During LST, single point calculations were carried out on the linearly interpolated structure on the minimum energy path joining the reactant and the product states. The state corresponding to the maximum energy along this minimum energy path is considered as the TS. This TS structure of which was taken as an intermediate for QST optimization, resulting into a more refined structure closer to the geometry of the activated complex. The obtained geometries of the TS for different reaction steps were further iterated using 'TS Optimization' module in DMol^3 to achieve refined TS structures. The vibrational frequencies of TS were analyzed and confirmed to be all real except one imaginary in the direction of the reaction coordinate. Both geometry optimization and transition state calculations were performed with the spin-polarized setup. Computations of the atomic charges for the reactant and the TS were performed by the Mulliken population analysis[30]. The initial structure of the Mo_4C_2 and Mo_2C_6 clusters were adapted from the work by Gao et al.[19]. Activation energies (E_a) were calculated as the difference in the energy between the transition and initial

states,

$$E_a = E_{TS} - E_{IS} \quad (1)$$

Where E_{TS} and E_{IS} represents the transition and initial state energies, respectively.

Adsorption energy of the intermediate species (E_{ads}) and surface reaction energies (E_r) of the elementary steps were calculated fromthe following equations;

$$E_{ads} = E_{mol+sur} - (E_{mol} + E_{sur}) \quad (2)$$

$$E_r = E_{FS} - E_{IS} \quad (3)$$

where $E_{mol+sur}$, E_{mol}, E_{sur} are energies of the adsorbed species on the cluster, molecule in the gas phase and the cluster, respectively. E_{IS}, E_{FS} are energies of the initial and final states of the reaction, respectively.

A comparison between the choice of exchange correlation functionals was performed on calculating the energetics of CH_4 dehydrogenation and C-C coupling reactions on Mo_4C_2 and Mo_2C_6 clusters using the Revised Perdew-Burke-Ernzerhof (RPBE) functional[31]. As presented in Table SI-1, both PW91 and RPBE functional followed the same trends, wherein RPBE systematically estimated a slightly higher activation barrier (≤ 10 kJ/mol) compared to the PW91 functional. It has to be further emphasized that DFT and higher level computational methods like CCSD(T) though give the same trends in most of the system, there can be few cases where differences may appear, as shown by Schaugaard et al.[32], wherein study was performed on the molybdenum oxide cluster. In their study, CCSD(T) was used to benchmark the data and DFT functionals were modified to tally the CCSD(T) data. Interestingly, DFT functional B3LYP gave the same trend to CCSD(T) method in all cases with one exception where it predicted a different ground state configuration.

Results and Discussion:

On a Mo_4C_2 cluster shown in Figure 1a, there were two types of Mo sites for CH_4 activation, $Mo^{(1)}$-C^{Mo} where Mo atom was coordinated with the two carbons and $Mo^{(2)}$-C^{Mo}, wherein Mo atom was coordinated with the one carbon. On the $Mo^{(1)}$-C^{Mo} site, the C-H activation barrier was calculated to be lower (116 kJ/mole), than that of $Mo^{(2)}$-C^{Mo} site (151 kJ/mol, Figure SI-1)

suggesting that the first methane activation was likely to occur on the $Mo^{(1)}$-C^{Mo} site. The reactant, TS and product geometries are shown in Figure 1b (a′ to b′) respectively. Adsorption of methane over the $Mo^{(1)}$ site occurred at a distance of 2.58 Å, Figure 1b (a′). In the activated complex shown in Figure 1b (CH_3-H^{TS}), both the CH_3 species and H atom remained bonded to the $Mo^{(1)}$ atom. The CH_3-$Mo^{(1)}$, H-$Mo^{(1)}$ and H-C^{Mo} bonds were 2.31 Å, 1.88 Å and 1.37 Å, respectively, whereas the internal CH_3-H bond distance was elongated to 1.66 Å. In the product state (Figure 1b, b′) the CH_3-H bond was broken, and H was completely transferred to the C^{Mo} site (H-C^{Mo} bond length 1.11 Å), while CH_3 remained bonded to the $Mo^{(1)}$ atom (CH_3-$Mo^{(1)}$ bond length 2.13 Å). Interaction of the CH_4 to the Mo_xC_y cluster have been studied by Zhou et al.[33]. As the CH_4 molecule approached the Mo center of the Mo_xC_y cluster, the electrons of the C-H bond were partly transferred to the LUMO of the Mo_xC_y cluster which mainly consists of the vacant d-orbitals of the Mo atom just above the Fermi level, subsequently leading to the C-H bond activation. On the same $Mo^{(1)}$-C^{Mo} site and cluster anchored on the Al-site of the zeolite, Gao et al. have calculated an activation barrier of 112 kJ/mol[7]. Since methane dehydrogenation activation energy on the isolated Mo_4C_2 was comparable to the one reported for the same cluster, anchored on the zeolite framework, rest of the calculations in this study on isolated clusters can be considered indicative of the trends, which may be obtained from corresponding supported clusters. Geometry for the TS obtained for methane C-H activation on Mo_4C_2 cluster was observed to be similar to the structures of the TS, previously observed for methane activation over the (111) and (211) surfaces of transition metals and as well as on the Pt_{79} cluster[35–38]. Methane C-H bond activation barrier obtained for Mo_4C_2 was comparable to activation barriers observed by Wang et al.[35] over the (111) surface of the transition metals; Pt, Pd, Rh and Ni (102, 109, 104 and 123 kJ/mol, respectively) and as well as on the (211) surface of Ni (109 kJ/mol). Activation barriers obtained for Pt, Pd and Rh (211) surfaces reported in previous studies (70, 80 and 64 kJ/mol, respectively) were lower than the one obtained for the Mo_4C_2, likely due to the presence of under coordinated edge sites. In comparison, methane C-H bond activation barriers reported by Zhu et al. over transition metal sulfide catalysts, MoS_2, RuS_2, PdS, and TiS_2 were significantly higher (> 150 kJ/mol)[39] than the one obtained on Mo_4C_2.

The second methane molecule had three choices as possible sites for activation; (1) same $Mo^{(1)}$ site where the first CH_3 was attached (Figure SI-2, c′ to d′), (2) free $Mo^{(1)}$ site (Figure SI-3, c‴ to d‴) and (3) free $Mo^{(2)}$ site (Figure SI-4, c⁗ to d⁗). Since barriers for CH_3 diffusion from the

neighboring $Mo^{(1)}$ site (197 kJ/mol, Figure SI-5a) and the second methane activation at the $Mo^{(2)}$ site (136 kJ/mol, Figure SI-5b) were calculated to be relatively higher as compared to the second methane activation at the same $Mo^{(1)}$ site, the same $Mo^{(1)}$ was considered most suitable for the second methane activation and subsequent C-C coupling, which is included in the reaction diagram shown in Figure 2 (c′ to d′). At the same $Mo^{(1)}$ atom, the second methane molecule was activated with an activation barrier of 117 kJ/mole, Figure 2 (c′ to d′). The H abstracted from the second methane molecule was adsorbed to the adjacent free carbon atom of the Mo_4C_2 cluster as shown in Figure SI-2 (c′ to d′).

The reaction proceeded through C-C coupling of the two adsorbed CH_3 groups with a 151 kJ/mole activation energy barrier and 43 kJ/mole intrinsic reaction energy to produce C_2H_6 (Figure 2, d′ to e′). Geometries of the reactant, TS and product states for the coupling of the two CH_3 over the $Mo^{(1)}$ site are shown in Figure 3a (d′ to e′). The Mo-C bond distance of the two adsorbed CH_3 groups were 2.20 Å and 2.21 Å, and the interatomic C-C bond distance between the two CH_3 groups was 2.95 Å, as shown in Figure 3a (d′). At the TS, the interatomic C-C bond length was shortened to 1.96 Å, whereas in the product state the formation of ethane was complete with a C-C bond length of 1.53 Å, Figure 3a (e′). Ethane was adsorbed weakly to the Mo_4C_2 cluster with the $Mo^{(1)}$-C^{Mo} distance calculating 2.52 Å and 2.93 Å, as shown in Figure 3a (e′). The geometry of the TS obtained for C-C coupling reaction of adsorbed CH_3 groups over the Mo_4C_2 cluster resembled closely to the TS structures reported for the C-C coupling reactions on the (111) and (211) surfaces of the transition metals in which the CH_x (x = 1, 2, 3) groups are generally observed bonded to two different surface atoms in the TS. The C-C coupling activation barriers obtained by Chen et al. [40] over the Pd(111) surface (E_a= 163 kJ/mol) was similar to the barrier obtained for Mo_4C_2 cluster. In contrast, the activation barrier for the coupling of the two CH_3 species over the (001) surface of Mo_2C surface (E_a = 106 kJ/mol) obtained by Medford et al.[41], was comparatively lower. Furthermore, the configuration of the activated complex for C-C coupling, obtained over the Mo_4C_2 cluster was similar in structure of the same step, observed over organometallic complexes of $Pd(CH_3)_2(PH_3)_2$ and $Pt(CH_3)_2(PH_3)_2$ by Ananikov et al.[42], wherein CH_3 groups were attached to the Pd or Pt atom. The C-C coupling activation barriers obtained for Pd and Pt organometallic systems were reported to be 101 and 187 kJ/mol, respectively[42].

The two adsorbed H were desorbed as H_2 gas in subsequent steps, first through H shifting from the neighboring carbons to the $Mo^{(2)}$ atom with an activation barrier of 107 kJ/mol (Figure 2, e′ to f′) and second by the formation of H_2 molecule through H-H coupling step of the hydrogen atoms adsorbed at the neighboring Mo and C with a similar activation energy barrier of 114 kJ/mole (Figure 2, f′ to g′). Geometries of the H-transfer (e′ to f′) and H-H coupling (f′ to g′) steps discussed above are shown in Figure 3b. Adsorbed H_2 was desorbed from the surface with a desorption energy of 48 kJ/mol (Figure 2, g′ to h′). Weakly adsorbed ethane molecule underwent subsequent activation at $Mo^{(1)}$ via two stepwise C-H bond dissociation with an activation energy of 70 kJ/mole (Figure 2, h′ to i′) and 95 kJ/mol (Figure 2, i′ to j′). Ethylene species thus formed was likely to diffuse to the active sites of the metal-support structure for subsequent steps to yield aromatics.

Apart from the Mo_4C_2, Mo_2C_6 cluster shown in Figure 4a was the other choice to study C-H activation and C-C coupling. Methane activation barrier over the $Mo^{(1)}$-C^{Mo} site, having an adjacent carbon from the C-C-C-C chain of the cluster, was calculated to be 194 kJ/mol (Figure SI-6). Compared to this, activation barrier for methane dehydrogenation on the $Mo^{(1)}$-C^{Mo} site present in the $Mo^{(1)}$-C^{Mo} - $Mo^{(1)}$-C^{Mo} plane of the cluster, was calculated to be lower (119 kJ/mol). The reactant, TS and product geometries corresponding to this C-H activation over the $Mo^{(1)}$-C^{Mo} site of the $Mo^{(1)}$-C^{Mo} - $Mo^{(1)}$-C^{Mo} plane are shown in Figure 4b (a″ to b″). Adsorption of methane over the $Mo^{(1)}$ site occurred at a distance of 2.78 Å as depicted in Figure 4b (a″). Adsorbed methane was activated with the CH_3 and the H species bonded to the $Mo^{(1)}$ atom at the TS, shown in Figure 4b (CH_3-H^{TS}). At the TS, CH_3-$Mo^{(1)}$, H-$Mo^{(1)}$ and H-C^{Mo} bond lengths were measured to be 2.35 Å, 1.84 Å and 1.37 Å, respectively, whereas the internal CH_3-H bond length was elongated to 1.60 Å. In the product state (Figure 4b, b″) the CH_3-H bond was broken, and H was completely transferred to the adjacent carbon (H-C bond length 1.10 Å) while CH_3 remained bonded to the $Mo^{(1)}$ atom (CH_3-$Mo^{(1)}$ bond length 2.16 Å). Geometry of the TS obtained for the C-H activation of methane on the Mo_2C_6 was observed to be similar to the geometry obtained for the previously described Mo_4C_2 cluster with comparable activation barrier.

In the TS, a similar multicenter bonding between activated CH_3-H and Mo-C^{Mo} active site was observed for both $Mo_4Ç_2$ and Mo_2C_6 clusters. The transition state of CH_3-H was stabilized by the transfer of an electron from the HOMO (filled d orbital just below the Fermi level) of the Mo_xC_y cluster to the anti-bonding states of the C-H bond. Among the two clusters, Mo_4C_2 had higher

electron density compared to Mo_2C_6 which may be attributed to greater stabilization of the transition state for methane dehydrogenation (given in Table 1) and hence calculating lower activation energy. For very similar reason Mo_4C_2 showed stronger binding to dissociated CH_3 and H, as evident in higher dissociated chemisorption values in Table 1. The transition states for methane dehydrogenation followed a linear scaling relationship with its corresponding dissociated chemisorption energy as shown in Figure 5. Similar linear transition state energy scaling with the dissociated chemisorption energy had been observed previously by Wang et al.[35] for CH_4 activation over transition metal surfaces. In a separate calculation, the activation barriers for dehydrogenation of methane over the Mo-Mo site were found to be unfavorable on both clusters. Table 2 shows the comparison of activation energies of the first C-H bond activation over the Mo-Mo sites on the two clusters as compared to the Mo-C^{Mo} sites. The underline reason for this high activation energy could be the longer Mo-Mo bond distances (Figure SI-7) as compared to the Mo-C^{Mo} bond distances (Figure 1b (CH_3-H^{TS}) for Mo_4C_2 and Figure 4b (CH_3-H^{TS}) for Mo_2C_6) in respective clusters resulting into less stable activated complex structures of methane undergoing dehydrogenation. Following the same reasoning of difficult CH_3 diffusion between different Mo sites, the second methane was activated over the same $Mo^{(1)}$ atom for subsequent C-C coupling (Figure SI-8). Energetics of this intrinsic step was calculated to be higher (E_a = 182 kJ/mol, and ΔH = 102 kJ/mol, Figure 6, c″ to d″), as compared to the first CH_3 activation (E_a = 119 kJ/mol, Figure 6, (a″ to b″), likely due to the steric and electronic effects of the first CH_3 species adsorbed on the same site. The C-C coupling reaction to form an adsorbed C_2H_6 on the surface occurred readily with an activation energy of 34 kJ/mol, Figure 6 (d″ to e″). Corresponding structures of the reactant, transition and product states are shown in Figure 7a (d″ to e″). The TS for the C-C coupling reaction on the Mo_2C_6 nanocluster was similar to the one obtained for Mo_4C_2 cluster. In the reactant state (Figure 7, d″), the Mo-C bond distance of the two adsorbed CH_3 groups was calculated to be 2.18 Å and 2.29 Å, and the interatomic C-C bond distance between the two CH_3 groups was 2.73 Å. For C-C coupling, at the TS, Figure 7a (CH_3-H^{TS}), the interatomic C-C bond length was shortened to 2.14 Å while both the CH_3 groups were bonded to the same $Mo^{(1)}$ atom. The product ethane was weakly adsorbed away from the Mo_2C_6 cluster, with elongated $Mo^{(1)}$-C bonds (2.93 Å and 2.65 Å) as shown in Figure 7a (e″). Subsequent formation of H_2 (g) occurred in two steps; the H was diffused from one Mo atom to the other with an activation barrier of 116 kJ/mol and reaction energy of 72 kJ/mol, Figure 6 (e″

to f″), followed by the coupling of adjacent hydrogen atoms adsorbed at neighboring C and $Mo^{(1)}$ to form the H_2(g) with an activation barrier of 136 kJ/mol and reaction energy 31 kJ/mol, Figure 6 (f″ to g″). Geometries of the H-transfer and H-H coupling steps discussed above are shown in Figure 7b. Similar to Mo_4C_2, the ethane molecule was further activated at $Mo^{(1)}$ site of the Mo_2C_6 cluster with an activation barrier of 130 kJ/mol to form C_2H_5, and subsequently with an activation barrier of 132 kJ/mol to form the desired product C_2H_4 as shown in Figure 6 (g″ to h″ and h″ to i″ respectively).

Depending on the anchoring site of the cluster, which may in-turn follow from the time-on-stream[7], the reduced state of the cluster is likely to vary. In order to study the effect of residual electron charge on the activity of the Mo_xC_y cluster, DFT calculations were employed for the two clusters; Mo_4C_2 and Mo_2C_6 with +1 charge. The origin of charge in molybdenum carbide (Mo_xC_y) or molybdenum oxy-carbide (MoO_xC_y) clusters have been explained by Iglesia, Beale, and co-workers[14,17,43]. During the carburization process, the residual charge remained on the MoC_x species was suggested to be an important factor influencing cluster-support interactions. Interestingly, neutral carbide cluster was suggested to bind loosely to the zeolite and may diffuse out of the zeolite channel leading to the formation of large nanoparticles and consequent catalyst deactivation[17]. Prior studies on methane activation have utilized similar isolated and charged clusters as the model for studying catalysis on metal with support. For example, Mowbray et al.[34] studied CH_4 and O_2 adsorption on TiO_2 supported transition metal catalysts by utilizing clusters of Au_n (n = 2, 6, 7, 49, 55, 155 and 201) and M_2 (M = Pt, Ir, Ag, Pd, Rh, Cu, and Ni) with varying charges. The author obtained a linear correlation between CH_4 and O_2 adsorption energy and the charge on the metal cluster. The reaction diagram for C-H activation and C-C coupling to form adsorbed ethylene on the +1 charge Mo_4C_2 nanocluster is shown in Figure 8. On the +1 charge Mo_4C_2, the methane dehydrogenation activation energy (142 kJ/mol, Figure 8, a′ to b′) was calculated to be higher by 26 kJ/mol as compared to the neutral cluster. Similarly, as compared to the first methane activation, the second methane C-H activation over the Mo_4C_2 cluster with +1 charge was calculated higher (131 kJ/mol, Figure 8, c′ to d′). In contrast, the activation barrier for CH_3-CH_3 coupling of the two adsorbed CH_3 groups at the $Mo^{(1)}$ to form C_2H_6, was reduced from 151 kJ/mol for the neutral Mo_4C_2 cluster to 63 kJ/mol for the +1 charge cluster, as shown in Figure 8 (d′ to e′). Similar to the trend in C-H activation, activation barriers for H_2 formation and dehydrogenation of C_2H_6 were observed to be increased for the +1 charge

Mo_4C_2 cluster. For this cluster, first the H adsorbed at the C atom was transferred to the $Mo^{(1)}$, with an activation barrier of 177 kJ/mol (Figure 8, e′ to f′) then hydrogen atoms adsorbed at the neighbouring C^{Mo} and $Mo^{(1)}$ were coupled to form H_2 with a smaller activation barrier of 82 kJ/mol (Figure 8, f′ to g′), which was similar to the mechanism observed for neutral Mo_4C_2 cluster. C_2H_6 adsorbed at $Mo^{(1)}$ was activated further in two steps, as shown in Figure 8, to form C_2H_4, with relatively higher C-H activation barriers; 183 kJ/mol (Figure 8, h′ to i′) and 100 kJ/mol (Figure 8, i′ to j') as compared to the corresponding neutral cluster.

The changes in energy profile for Mo_2C_6 cluster with the +1 charge followed the same trend with few exceptions. The corresponding reaction diagram is presented in Figure 9. Methane activation barrier for +1 charge (133 kJ/mol, Figure 9, a″ to b″) was 14 kJ/mol higher than that of the neutral cluster. The second methane dissociation (Ea= 181 kJ/mol, Figure 9, c″ to d″), however; was similar to the neutral Mo_2C_6 cluster. Interestingly, the C-C coupling of two adsorbed CH_3 at $Mo^{(1)}$ was reduced to a negligible barrier (Figure 9, d″ to e″). The activation barrier for H-H coupling to yield H_2 decreased relatively as compared to the neutral cluster. Similar to the neutral cluster, in the first step, H adsorbed at C^{Mo} was moved to $Mo^{(1)}$, before the coupling of H atoms Figure 9 (e″ to f″). This step was highly endothermic with intrinsic reaction energy of 133 kJ/mol. In the second step, the two hydrogen atoms adsorbed at neighboring $Mo^{(1)}$ and C^{Mo} combined to form H_2 at the $Mo^{(1)}$ site, with an activation barrier of 113 kJ/mol, as shown in Figure 9 (f″ to g″). The ethane molecule formed at the $Mo^{(1)}$ site was activated further to give ethylene in two subsequent steps through C-H bond activation, with activation energies of 140 kJ/mol (Figure 9, g″ to h″) and 109 kJ/mol (Figure 9, h″ to i″). While the activation barrier for C_2H_6 dehydrogenation was increased by 10 kJ/mol, it was decreased by 23 kJ/mol for subsequent C_2H_5 dehydrogenation, on the +1 charge Mo_2C_6 as compared to the neutral cluster, On comparing the two reaction diagrams (Figure 9 and Figure 8), it can be deduced that first the methane dehydrogenation was relatively easier on the +1 charge Mo_2C_6 cluster as compared to the +1 charge Mo_4C_2 cluster. However, second methane activation was difficult on the +1 charge Mo_2C_6 cluster. Moreover, C-C and H-H coupling became even more facile on the +1 charge Mo_2C_6 cluster as compared to the +1 charge Mo_4C_2 cluster. Since C-H bond activation is considered to be rate determining in most MDA studies[44], an analysis of first methane dehydrogenation with increasing cluster charge was performed. Figure 10 shows the C-H bond activation energies of methane plotted versus 0, +1, +1.5 and +2 charge Mo_4C_2 and Mo_2C_6 clusters. Methane

dehydrogenation barrier was observed to decrease as the Mo_xC_y clusters were more reduced. In general, for the same cluster charge, first methane activation barrier over the Mo_2C_6 cluster was calculated lesser than that of the Mo_4C_2 cluster for all the charges studied here, except for the neutral charge, where activation energy values were comparable. The result obtained correlated with the experimental findings showing better reducibility of the Mo_xC_y clusters responsible for higher methane conversion[45].

An inference to the increase in C-H bond activation barriers with the increase in cluster residual charge on the respective clusters is obtained from the Mulliken charge distribution, and analysis shown in Figure 11 and Table 3 respectively for the two different charges (neutral and +1) applied to the two clusters. With an increase in cluster charge, the Mo sites became more positive and hence less active for C-H bond activation. With few exceptions, likely due to the geometric effects, this was true for C-H bond activation in the first CH_4, second CH_4, C_2H_6 and C_2H_5 species on the respective Mo_4C_2 and Mo_2C_6 clusters. Since the coordination geometry varies between the two clusters a similar interpretation to C-H bond activation energy trend between the two clusters may not apply. Only for C-H bond activation in C_2H_5 on the Mo_2C_6 the dehydrogenation barrier was observed to decrease (from 132 kJ/mol (Figure 6) to 109 kJ/mol (Figure 9) on increasing the cluster residual charge from neutral to +1. To explain this, the transition state geometry of C_2H_5 activation on both neutral and +1 charge Mo_2C_6 clusters were compared, as shown in Figure SI-9. For the neutral charge cluster, the ethylene molecule is closer towards the Mo_2C_6 cluster, with Mo-C bond lengths (2.37 Å and 2.25 Å), while the C=C bond lengths were elongated (1.44 Å). Similarly, the TS obtained for the +1 charge cluster is significantly different from the corresponding structures of the TS in the neutral cluster. In the TS, for the +1 charge Mo_2C_6 cluster, the C_2H_4 group is further away from the Mo center, with Mo-C bond lengths calculating 2.51 Å and 2.42 Å and shorter C=C bond length calculating 1.38 Å. Since the final state of the dehydrogenation reaction (C_2H_4+2H) is more stable for the +1 charge cluster (-5 kJ/mol, Figure 9, i″), compared to the neutral Mo_2C_6 cluster (78 kJ/mol, Figure 6, i″), the final state like TS for +1 charge cluster is stabilized further, causing a decrease in the activation barrier.

For the CH_3-CH_3 coupling at the same Mo site, the activation energy correlates well with the binding energy trend of the CH_3 species at the respective cluster as shown in Table 1. Lesser the binding energy of the CH_3 species, easier was the C-C coupling reaction. However, this may not

hold true for H-H coupling to form H_2, since H-H coupling occurred from two different sites (neighboring C^{Mo} and Mo), which might introduce a geometric dependence. A better descriptor to explain the activation trend in C-H bond and C-C coupling reactions on these carbide clusters is desirable. Previous attempts by Nørskov and co-workers for metal carbide have shown limitations in search of a suitable descriptor for the surface reactivity of metal carbides as compared to pure transitions metal surface.[46,47] Lundqvist and co-workers proposed surface resonance as a better descriptor for explaining the binding energy trends than the conventional d-band center model for carbides and nitrides.[48–52] In addition, for the cluster, the coordination geometry[53–55] is expected to play a greater role in determining reactivity.

In separate studies by Zhu et al.[39] and Guo et al.[56], two alternative pathways for C-H activation and C-C coupling were discussed which were primarily based on the activation of adsorbed CH_3 groups to form CH_2, which subsequently underwent C-C coupling to form ethylene[39] or the formation of CH_3 radical through desorption of adsorbed CH_3 and formation of C_2H_6 in gas phase through CH_3 radical coupling[56]. These two pathways are shown in scheme (b) and (c), respectively, in Figure SI-10. In the same Figure, scheme (a) represents the mechanism discussed in detail above. Following scheme (b), the C-H activation barriers of the adsorbed CH_3 groups to form CH_2 and H, was calculated to be higher; 169 kJ/mol (Figure SI-11) and 294 kJ/mol (Figure SI-11) for the 1st and 2nd CH_3, respectively on the Mo_2C_4 cluster and 153 kJ/mol (Figure SI-12) for the 2nd CH_3 activation on the Mo_2C_6 cluster, hence this pathway was considered unlikely. Similarly, following scheme (c) the desorption barriers for adsorbed CH_3 groups to gas-phase was calculated to be high (E_a=301 kJ/mol) on the Mo_4C_2 (Figure SI-13) and (E_a= 246 kJ/mol) on the Mo_2C_6 cluster (Figure SI-14), which ruled out the radical initiation pathway. It is consistent with the reported CH_3 radical desorption barriers (224 kJ/mol) by Guo et al. on FeC_2 active center embedded in a SiO_2 support matrix.[56] In the product state C_2H_4 was adsorbed to the molybdenum carbide cluster and depending on the adsorption energy of C_2H_4 at the carbide cluster, the reaction energy was changed. The C_2H_4 formed on the cluster will further diffuse to the Brønsted acid site of the zeolite where the chain elongation and aromatization steps will occur as suggested by Ismagilov et al., Ichikawa et al. and Iglesia et al.[2,13,57] Thus it can be concluded that the formation of ethylene, which is an important intermediate for the aromatics formation, is likely to proceed through the formation of ethane via CH_3-CH_3 coupling and subsequent C-H activation as discussed in this study.

Conclusions

The reducibility of the Mo/zeolite catalyst is a key factor determining the catalyst activity. Herein, DFT calculations were performed to study the effect of charge on catalytically active carbide (Mo_xC_y) clusters in C-H bond activation and C-C coupling reactions to form ethylene. A detailed mechanistic understanding, correlating the effect of charge to catalyst activity was developed, which may help in providing guidelines on controlling the structure of the Mo species in obtaining the desired product with increased catalyst stability. A linear correlation between the cluster residual charge and first barrier for methane dehydrogenation was obtained, wherein the lesser residual charge on the Mo_xC_y cluster dictated lowering of the methane dehydrogenation barrier. For example, CH_3-H activation was calculated to be 116 kJ/mol and 173 kJ/mol for the neutral and the +2 charge Mo_4C_2 cluster, respectively. Residual charge on the Mo_xC_y clusters showed a distinct effect on the energy diagrams obtained for methane conversion to ethylene.

C-H bond activation barriers for both methane and ethane were increased for +1 charge Mo_4C_2 and Mo_2C_6 clusters, whereas C-C coupling reaction was facilitated on the higher charge cluster. Between the two clusters, Mo_2C_6 showed significantly lower activation barriers for C-C coupling reaction step. However, second methane dehydrogenation was calculated to be difficult on Mo_2C_6 cluster. Therefore, it can be concluded that while methane may be activated on both clusters, C-C coupling and subsequent formation of aromatics is likely to occur with a synergistic interaction of the Mo_2C_6 cluster and neighboring Brønsted acid sites of the support, as also proposed by Beale, Weckhuysen, and co-workers.[17] However, these results should be interpreted with two important limitations. One is related to the spin state of the isolated clusters, which may influence the energetics as shown in the work of Sheng-Gui He and co-workers[58–62] and second is related to the structure of the cluster. Interestingly, methane dehydrogenation calculations by Gao et al., [*Science* **2015**, *348*, 686-690] on a Mo_4C_2 cluster, anchored on a zeolite framework had assumed a cluster structure which was optimized at a neutral charge. The cluster-support interaction is likely to influence the stability of the cluster itself.

Nevertheless, the results are applied to the future development of the MDA process, wherein catalyst stability and low activity are the two main factors hindering the prospects of commercialization. The activity of the catalyst may be increased by stabilizing the cluster charge formed under the reaction condition, to generate the important ethylene intermediate. Moreover,

reducibility of the catalyst may be controlled during the catalyst preparation or regeneration steps. While a more reduced catalyst showed better C-H bond activation, the C-C coupling reactions was favored over the charged clusters. Therefore, in the design of the MDA process, optimization of the charge on the Mo_xC_y clusters is important, which may in-turn also improve catalyst stability. In this direction, the choice and use of an appropriate dopant could be a way forward.

Acknowledgments

Authors would like to thank the IIT Delhi HPC facility for the computational resource. Financial support from Gas Authority of India Limited (GAIL (INDIA) Ltd.) is appreciated.

Associated Content:

Supporting information contains a comparison of exchange-correlation functionals, effect of cluster charge on an intermediate species (CH_3^*) binding energies over the two clusters and the reaction energetics following scheme (b) and (c).

References

(1) Spivey, J. J.; Hutchings, G. Catalytic Aromatization of Methane. *Chem. Soc. Rev.* **2014**, *43*, 792–803.

(2) Ismagilov, Z. R.; Matus, E. V.; Tsikoza, L. T. Direct Conversion of Methane on Mo/ZSM-5 Catalysts to Produce Benzene and Hydrogen : Achievements and Perspectives. *Energy Environ. Sci.* **2008**, 1, 526-541.

(3) Mcfarland, E. Unconventional Chemistry for Unconventional Natural Gas. *Science* **2012**, *338*, 340–343.

(4) Lunsford, J. H. Catalytic Conversion of Methane to More Useful Chemicals and Fuels: A Challenge for the 21st Century. *Catal. Today* **2000**, *63*, 165–174.

(5) Majhi, S.; Mohanty, P.; Wang, H.; Pant, K. K. Direct Conversion of Natural Gas to Higher Hydrocarbons: A Review. *J. Energy Chem.* **2013**, *22*, 543–554.

(6) Ma, S.; Guo, X.; Zhao, L.; Scott, S. Recent Progress in Methane Dehydroaromatization: From Laboratory Curiosities to Promising Technology. *J. Energy Chem.* **2013**, *22*, 1–20.

(7) Gao, J.; Zheng, Y.; Jehng, J.; Tang, Y.; Wachs, I. E.; Podkolzin, S. G. Identification of Molybdenum Oxide Nanostructures on Zeolites for Natural Gas Conversion. *Science* **2015**, *348*, 686-690.

(8) Khalilpour, R.; Karimi, I. A. Evaluation of Utilization Alternatives for Stranded Natural Gas. *Energy* **2012**, *40*, 317–328.

(9) Skutil, K.; Taniewski, M. Some Technological Aspects of Methane Aromatization (Direct and via Oxidative Coupling). *Fuel Process. Technol.* **2006**, *87*, 511–521.

(10) Shu, Y.; Ma, D.; Xu, L.; Xu, Y.; Bao, X. Methane Dehydro-Aromatization over Mo/MCM-22 Catalysts: A Highly Selective Catalyst for the Formation of Benzene. *Catal. Letters* **2000**, *70*, 67–73.

(11) Song, Y.; Zhang, Q.; Xu, Y.; Zhang, Y.; Matsuoka, K. Coke Accumulation and Deactivation Behavior of Microzeolite-Based Mo/HZSM-5 in the Non-Oxidative Methane Aromatization under Cyclic CH_4 -H_2 Feed Switch Mode. *Appl. Catal. A, Gen.* **2017**, *530*, 12–20.

(12) Ma, D.; Wang, D.; Su, L.; Shu, Y.; Xu, Y.; Bao, X. Carbonaceous Deposition on Mo/ HMCM-22 Catalysts for Methane Aromatization: A TP Technique Investigation. *J. Catal.* **2002**, *269*, 260–269.

(13) Ohnishi, R.; Liu, S.; Dong, Q.; Wang, L.; Ichikawa, M. Catalytic Dehydrocondensation of Methane with CO and CO_2 toward Benzene and Naphthalene on Mo/HZSM-5 and Fe/Co-Modified Mo/HZSM-5. *J. Catal.* **1999**, *103*, 92–103.

(14) Ding, W.; Li, S.; Meitzner, G. D.; Iglesia, E. Methane Conversion to Aromatics on Mo/H-ZSM5 : Structure of Molybdenum Species in Working Catalysts. *J. Phys. Chem. B* **2001**, *105*, 506–513.

(15) Solymosi, F.; Cserényi, J.; Szöke, A.; Bánsági, T.; Oszkó, A. Aromatization of Methane over Supported and Unsupported Mo-Based Catalysts. *J. Catal.* **1997**, *165*, 150–161.

(16) Liu, H.; Bao, X.; Xu, Y. Methane Dehydroaromatization under Nonoxidative Conditions over Mo/HZSM-5 Catalysts: Identification and Preparation of the Mo Active Species. *J. Catal.* **2006**, *239*, 441–450.

(17) Lezcano-González, I.; Oord, R.; Rovezzi, M.; Glatzel, P.; Botchway, S. W.; Weckhuysen, B. M.; Beale, A. M. Molybdenum Speciation and Its Impact on Catalytic Activity during Methane Dehydroaromatization in Zeolite ZSM-5 as Revealed by Operando X-Ray

Methods. *Angew. Chem., Int. Ed.* **2016**, *55*, 5215–5219.

(18) Li, B.; Li, S.; Li, N.; Chen, H.; Zhang, W.; Bao, X.; Lin, B. Structure and Acidity of Mo/ZSM-5 Synthesized by Solid State Reaction for Methane Dehydrogenation and Aromatization. *Microporous Mesoporous Mater.* **2006**, *88*, 244–253.

(19) Gao, J.; Zheng, Y.; Fitzgerald, G. B.; Joannis, J. De.; Tang, Y.; Wachs, I. E.; Podkolzin, S. G. Structure of Mo_2C_X and Mo_4C_X Molybdenum Carbide Nanoparticles and Their Anchoring Sites on ZSM‑5 Zeolites. *J. Phys. Chem. C* **2014**, *118*, 4670−4679.

(20) Liu, S.; Wang, L.; Ohnishi, R.; Ichikawa, M. Bifunctional Catalysis of Mo/HZSM-5 in the Dehydroaromatization of Methane to Benzene and Naphthalene XAFS/TG/DTA/MASS/ FTIR Characterization and Supporting Effects. *J. Catal.* **1999**, *188*, 175–188.

(21) Delley, B. An All-Electron Numerical Method for Solving the Local Density Functional for Polyatomic Molecules. *J. Chem. Phys.* **1990**, *92*, 508.

(22) Perdew, J. P.; Wang, Y. Accurate and Simple Analytic Representation of the Electron-Gas Correlation Energy. *Phys. Rev. B* **1992**, *45*, 244–248.

(23) Smit, E. De.; Cinquini, F.; Beale, A. M.; Safonova, O. V.; Beek, W. Van.; Sautet, P.; Weckhuysen, B. M.; Supe, N.; Horowitz, R. J.; Cedex, F. G. Stability and Reactivity of ε-χ-θ Iron Carbide Catalyst Phases in Fischer-Tropsch Synthesis : Controlling μC. *J. Am. Chem. Soc.* **2010**, *132*, 14928–14941.

(24) Yu, W.; Salciccioli, M.; Xiong, K.; Barteau, M. A.; Vlachos, D. G.; Chen, J. G. Theoretical and Experimental Studies of C-C versus C-O Bond Scission of Ethylene Glycol Reaction Pathways via Metal-Modified Molybdenum Carbides. *ACS Catal.* **2014**, *4*, 1409–1418.

(25) Zhu, R.; Hao, S.; Sholl, D. S. Selection of Surface Coatings for High H_2 Permeability Group 5 Metal Membranes Using First-Principles Calculations. *J. Phys. Chem. C* **2015**, *119*, 7848–7855.

(26) Vojvodic, A.; Ruberto, C. Trends in Bulk Electron-Structural Features of Rocksalt Early Transition-Metal Carbides. *J. Phys. Condens. Matter* **2010**, *22*, 375501.

(27) Park, N. Y.; Choi, J. H.; Cha, P. R.; Jung, W. S.; Chung, S. H.; Lee, S. C. First-Principles Study of the Interfaces between Fe and Transition Metal Carbides. *J. Phys. Chem. C* **2013**, *117*, 187–193.

(28) Viñes, F.; Sousa, C.; Illas, F.; Liu, P.; Rodriguez, J. A. Density Functional Study of the Adsorption of Atomic Oxygen on the (001) Surface of Early Transition-Metal Carbides. *J.*

Phys. Chem. C **2007**, *111*, 1307–1314.

(29) Halgren, T. A.; Lipscomb, W. N. The Synchronous-Transit Method for Determining Reaction Pathways and Locating Molecular Transition States. *Chem. Phys. Lett.* **1977**, *49*, 225–232.

(30) Mulliken, R. S. Electronic Population Analysis on LCAO–MO Molecular Wave Functions. I. *J. Chem. Phys.* **1955**, *23*, 1833–1840.

(31) Hammer, B.; Hansen, L. B.; Nørskov, J. K. Improved Adsorption Energetics within Density-Functional Theory Using Revised Perdew-Burke-Ernzerhof Functionals. *Phys. Rev. B* **1999**, *59*, 7413–7421.

(32) Schaugaard, R. N.; Topolski, J. E.; Ray, M.; Raghavachari, K.; Jarrold, C. C. Insight into Ethylene Interactions with Molybdenum Suboxide Cluster Anions from Photoelectron Spectra of Chemifragments. *J. Chem. Phys.* **2018**, *148*, 054308–054313.

(33) Zhou, T.; Liu, A.; Mo, Y.; Zhang, H. Sequential Mechanism of Methane Dehydrogenation over Metal (Mo or W) Oxide and Carbide Catalysts. *J. Phys. Chem. A* **2000**, *104*, 4505–4513.

(34) Mowbray, D. J.; Migani, A.; Walther, G.; Cardamone, D. M.; Rubio, A. Gold and Methane: A Noble Combination for Delicate Oxidation. *J. Phys. Chem. Lett.* **2013**, *4*, 3006–3012.

(35) Wang, S.; Petzold, V.; Tripkovic, V.; Kleis, J.; Howalt, J. G.; Skúlason, E.; Fernández, E. M.; Hvolbæk, B.; Jones, G.; Toftelund, A.; Falsig, H.; Björketun, M.; Studt, F.; Abild-Pedersen, F.; Rossmeisl, J.; Nørskov, J. K.; Bligaard, T. Universal Transition State Scaling Relations for (de)hydrogenation over Transition Metals. *Phys. Chem. Chem. Phys.* **2011**, *13*, 20760–20765.

(36) Grootel, P. W. Van; Santen, R. A. Van; Hensen, E. J. M. Methane Dissociation on High and Low Indices Rh Surfaces. *J. Phys. Chem. C* **2011**, *115*, 13027–13034.

(37) Nikolla, E.; Schwank, J.; Linic, S. Comparative Study of the Kinetics of Methane Steam Reforming on Supported Ni and Sn/Ni Alloy Catalysts: The Impact of the Formation of Ni Alloy on Chemistry. *J. Catal.* **2009**, *263*, 220–227.

(38) Viñes, F.; Lykhach, Y.; Staudt, T.; Lorenz, M. P. A.; Papp, C.; Steinrück, H.; Libuda, J.; Neyman, K. M.; Görling, A. Methane Activation by Platinum: Critical Role of Edge and Corner Sites of Metal Nanoparticles. *Chem. A Eur. J.* **2010**, *16*, 6530–6539.

(39) Zhu, Q.; Wegener, S. L.; Xie, C.; Uche, O.; Neurock, M.; Marks, T. J. Sulfur as a Selective "soft" Oxidant for Catalytic Methane Conversion Probed by Experiment and Theory. *Nat. Chem.* **2012**, *5*, 104–109.

(40) Chen, Z.; Aleksandrov, H. A.; Basaran, D.; Rösch, N. Transformations of Ethylene on the Pd(111) Surface: A Density Functional Study. *J. Phys. Chem. C* **2010**, *114*, 17683–17692.

(41) Medford, A. J.; Vojvodic, A.; Studt, F.; Abild-Pedersen, F.; Nørskov, J. K. Elementary Steps of Syngas Reactions on $Mo_2C(001)$: Adsorption Thermochemistry and Bond Dissociation. *J. Catal.* **2012**, *290*, 108–117.

(42) Ananikov, V. P.; Musaev, D. G.; Morokuma, K. Theoretical Insight into the C−C Coupling Reactions of the Vinyl, Phenyl, Ethynyl, and Methyl Complexes of Palladium and Platinum. *Organometallics* **2005**, *24*, 715-723.

(43) Li, W.; Meitzner, G. D.; Borry, R. W.; Iglesia, E. Raman and X-Ray Absorption Studies of Mo Species in Mo/H-ZSM-5 Catalysts for Non-Oxidative CH_4 Reactions. *J. Catal.* **2000**, *191*, 373–383.

(44) Karakaya, C.; Zhu, H.; Kee, R. J. Kinetic Modeling of Methane Dehydroaromatization Chemistry on Mo/Zeolite Catalysts in Packed-Bed Reactors. *Chem. Eng. Sci.* **2015**, *123*, 474–486.

(45) Shu, Y.; Xu, Y.; Wong, S.; Wang, L.; Guo, X. Promotional Effect of Ru on the Dehydrogenation and Aromatization of Methane in the Absence of Oxygen over Mo/HZSM-5 Catalysts. *J. Catal.* **1997**, *19*, 11–19.

(46) Kitchin, J. R.; Nørskov, J. K.; Barteau, M. A.; Chen, J. G. Trends in the Chemical Properties of Early Transition Metal Carbide Surfaces: A Density Functional Study. *Catal. Today* **2005**, *105*, 66–73.

(47) Fernández, E. M.; Moses, P. G.; Toftelund, A.; Hansen, H. A.; Martínez, J. I.; Abild-Pedersen, F.; Kleis, J.; Hinnemann, B.; Rossmeisl, J.; Bligaard, T.; Nørskov, J. K. Scaling Relationships for Adsorption Energies on Transition Metal. *Angew. Chem., Int. Ed.* **2008**, *47*, 4683–4686.

(48) Vojvodic, A.; Hellman, A.; Ruberto, C.; Lundqvist, B. I. From Electronic Structure to Catalytic Activity: A Single Descriptor for Adsorption and Reactivity on Transition-Metal Carbides. *Phys. Rev. Lett.* **2009**, *103*, 1–4.

(49) Ruberto, C.; Lundqvist, B. I. Nature of Adsorption on TiC(111) Investigated with Density-

Functional Calculations. *Phys. Rev. B* **2007**, *75*, 235438.

(50) Ruberto, C.; Vojvodic, A.; Lundqvist, B. I. Nature of Versatile Chemisorption on TiC(111) and TiN(111) Surfaces. *Solid State Commun.* **2007**, *141*, 48–52.

(51) Ruberto, C.; Vojvodic, A.; Lundqvist, B. I. Nature of Chemisorption on Titanium Carbide and Nitride. *Surf. Sci.* **2006**, *600*, 1612–1618.

(52) Vojvodic, A.; Ruberto, C.; Lundqvist, B. I. Atomic and Molecular Adsorption on Transition-Metal Carbide(111) Surfaces from Density-Functional Theory: A Trend Study of Surface Electronic Factors. *J. Phys. Condens. Matter* **2010**, *22*, 375504.

(53) Li, Z.; Ma, X.; Xin, H. Feature Engineering of Machine-Learning Chemisorption Models for Catalyst Design. *Catal. Today* **2017**, *280*, 232–238.

(54) Ma, X.; Xin, H. Orbitalwise Coordination Number for Predicting Adsorption Properties of Metal Nanocatalysts. *Phys. Rev. Lett.* **2017**, *118*, 1–5.

(55) Ma, X.; Li, Z.; Achenie, L. E. K.; Xin, H. Machine-Learning-Augmented Chemisorption Model for CO_2 Electroreduction Catalyst Screening. *J. Phys. Chem. Lett.* **2015**, *6*, 3528−3533.

(56) Guo, X.; Fang, G.; Li, G.; Fan, H.; Yu, L.; Wu, X.; Deng, D.; Wei, M.; Tan, D.; Si, R.; Zhang, S.; Li, J.; Sun, L.; Tang, Z.; Pan, X.; Bao, X. Direct, Nonoxidative Conversion of Methane to Ethylene, Aromatics, and Hydrogen. *Science* **2014**, *344*, 616–620.

(57) Richard W Borry; Lu, E. C.; Kim, Y.; Iglesia, E. Non-Oxidative Catalytic Conversion of Methane with Continuous Hydrogen Removal. *Stud. Surf. Sci. Catal.* **1998**, *119*, 403–410.

(58) Li, Z. Y.; Hu, L.; Liu, Q. Y.; Ning, C. G.; Chen, H.; He, S. G.; Yao, J. C-H Bond Activation by Early Transition Metal Carbide Cluster Anion MoC_3^-. *Chem. A Eur. J.* **2015**, *21*, 17748–17756.

(59) Liu, Q. Y.; Ma, J. B.; Li, Z. Y.; Zhao, C.; Ning, C. G.; Chen, H.; He, S. G. Activation of Methane Promoted by Adsorption of CO on $Mo_2C_2^-$ Cluster Anions. *Angew. Chem., Int. Ed.* **2016**, *55*, 5760–5764.

(60) Li, H. F.; Zhao, Y. X.; Yuan, Z.; Liu, Q. Y.; Li, Z. Y.; Li, X. N.; Ning, C. G.; He, S. G. Methane Activation by Tantalum Carbide Cluster Anions $Ta_2C_4^-$. *J. Phys. Chem. Lett.* **2017**, *8*, 605–610.

(61) Li, Z. Y.; Yuan, Z.; Zhao, Y. X.; He, S. G. Methane Activation by Diatomic Molybdenum Carbide Cations. *Chem. A Eur. J.* **2014**, *20*, 4163–4169.

(62) Li, H. F.; Li, Z. Y.; Liu, Q. Y.; Li, X. N.; Zhao, Y. X.; He, S. G. Methane Activation by Iron-Carbide Cluster Anions FeC_6^-. *J. Phys. Chem. Lett.* **2015**, *6*, 2287–2291.

Table 1. Dissociative chemisorption (E_{diss}) and TS (E_{TS}) energies of the first and second methane dehydrogenation steps on the respective two clusters with increasing charge.

Mo_4C_2			
$CH_4 \rightarrow CH_3^* + H^*$	Neutral	Charge +1	Charge +2
	E_{diss} (kJ/mol)		
First CH_4 dehydrogenation	-61.9	-49.4	-65.9
Second CH_4 dehydrogenation	-64.9	-35.9	-165.5
	E_{TS} (kJ/mol)		
First CH_4 dehydrogenation	79.9	131.9	83.7
Second CH_4 dehydrogenation	32.5	58.4	-35.2
Mo_2C_6			
$CH_4 \rightarrow CH_3^* + H^*$	Neutral	Charge +1	Charge +2
	E_{diss} (kJ/mol)		
First CH_4 dehydrogenation	-19.5	-58.5	-137.8
Second CH_4 dehydrogenation	70.5	34.5	-74.0
	E_{TS} (kJ/mol)		
First CH_4 dehydrogenation	90.4	68.9	7.8
Second CH_4 dehydrogenation	151.3	139.9	55

*dissociated CH_3 and H adsorbed at Mo and C^{Mo} atoms, respectively.

Table 2. Comparison of activation energy of methane C-H bond activation over Mo-Mo and Mo-C sites.

Activation site	Activation Energy (kJ/mol)	Mo-Mo (or Mo-C) bond length (Å)
Mo_4C_2		
CH_3 adsorbed at $Mo^{(1)}$ and H adsorbed at neighboring C^{Mo}	116	1.92
CH_3 adsorbed at $Mo^{(2)}$ and H adsorbed at neighboring C^{Mo}	151	2.19
CH_3 adsorbed at $Mo^{(1)}$ and H adsorbed at $Mo^{(1)}$	228	2.82
CH_3 adsorbed at $Mo^{(1)}$ and H adsorbed at $Mo^{(2)}$	184	2.40
Mo_2C_6		
CH_3 adsorbed at $Mo^{(1)}$ and H adsorbed at neighboring C^{Mo}	119	1.90
CH_3 adsorbed at $Mo^{(1)}$ and H adsorbed at $Mo^{(1)}$	379	2.69

Table 3. Mulliken charge analysis for Mo_4C_2 and Mo_2C_6 clusters corresponding to electron density profiles shown in Figure 11.

Mo_4C_2	**Mulliken Charge**		**ΔCharge**
Atoms	Neutral	Charge(+1)	
$Mo^{(1)}$	0.442	0.631	0.189
$Mo^{(1)}$	0.398	0.594	0.196
$Mo^{(2)}$	0.134	0.385	0.251
$Mo^{(2)}$	0.151	0.386	0.235
C^{Mo}	-0.565	-0.500	0.065
C^{Mo}	-0.560	-0.496	0.064

Mo_2C_6	**Mulliken Charge**		**ΔCharge**
Atoms	Neutral	Charge(+1)	
$Mo^{(1)}$	0.644	0.838	0.194
$Mo^{(1)}$	0.632	0.821	0.189
C^{Mo}	-0.413	-0.309	0.104
C^{Mo}	-0.413	-0.308	0.105
C^{Mo}	-0.295	-0.188	0.107
C^{Mo}	-0.003	0.11	0.113
C^{Mo}	0.102	0.197	0.095
C^{Mo}	-0.255	-0.16	0.095

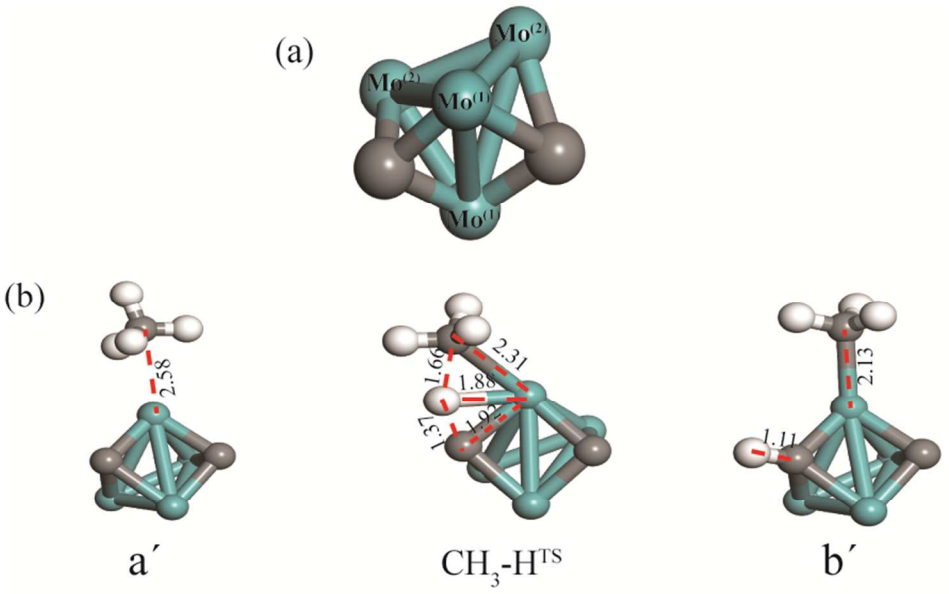

Figure 1. Geometry of (a) the Mo_4C_2 cluster and (b) reactant, transition and product states for methane dehydrogenation over the $Mo^{(1)}$ site. (bond lengths in Å)

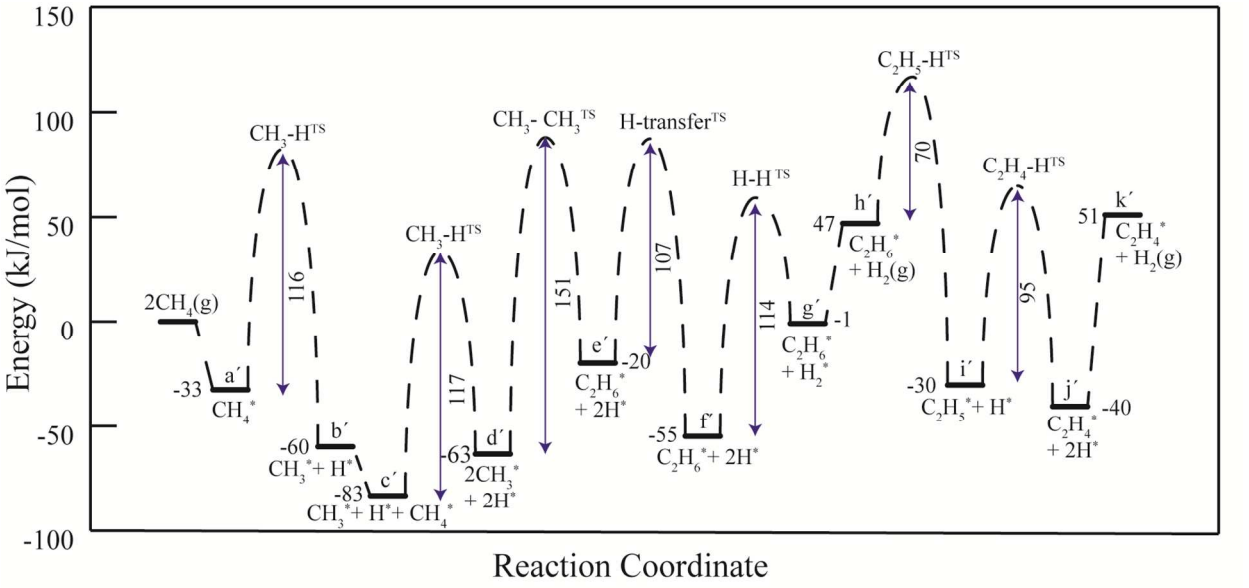

Figure 2. Reaction diagram for methane dehydrogenation and C-C coupling reactions to form ethylene on Mo_4C_2 cluster.

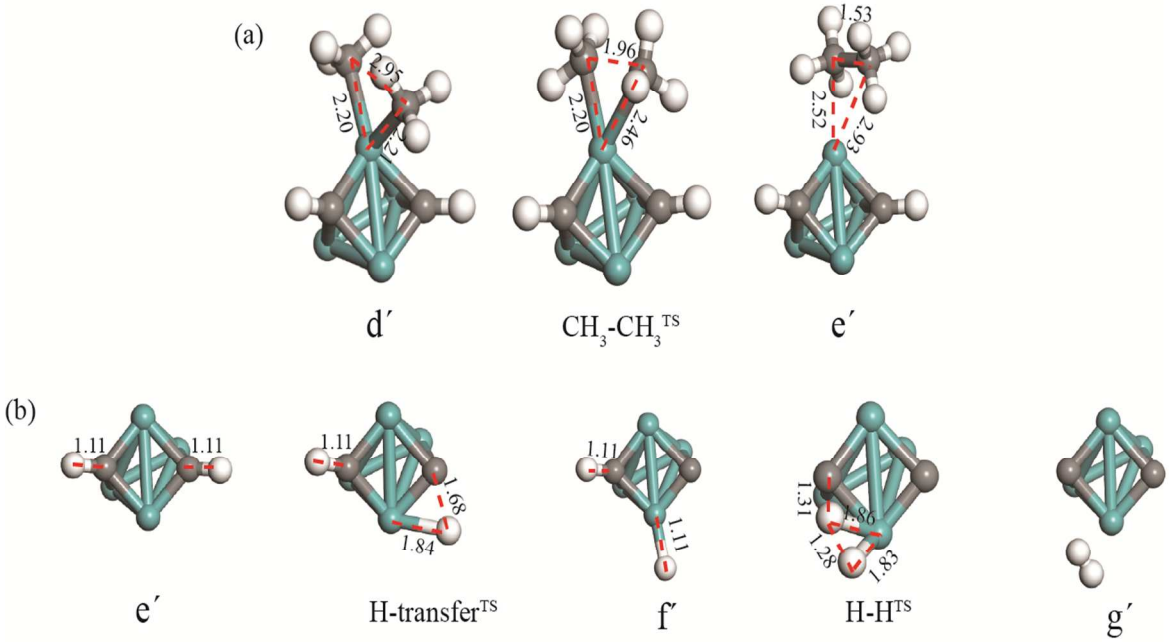

Figure 3. Geometry of the reactant, transition and product states for (a) coupling of the two CH_3 species and (b) H_2 formation reaction steps over Mo_4C_2 Nano cluster. (bond lengths in Å)

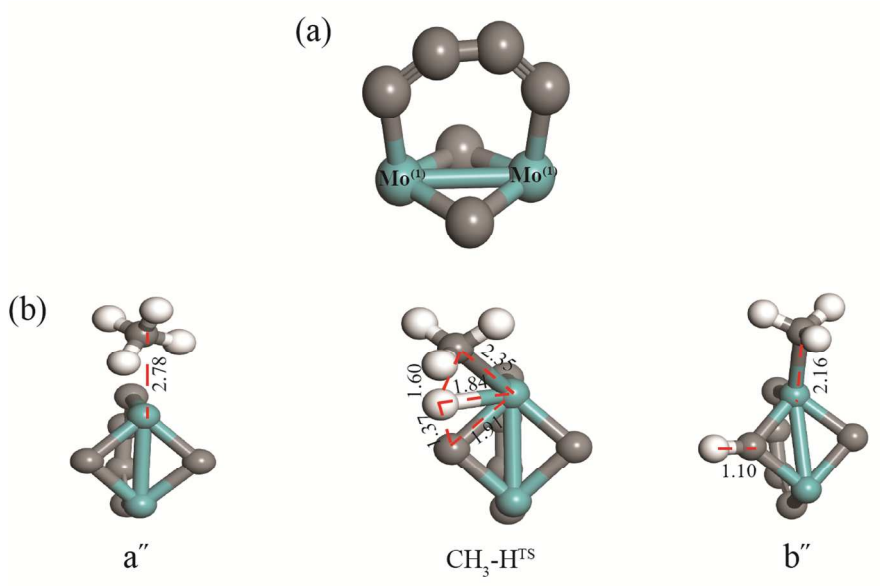

Figure 4. Geometry of (a) the Mo_2C_6 cluster and (b) reactant, transition and product states for methane dehydrogenation over the $Mo^{(1)}$ site. (bond lengths in Å).

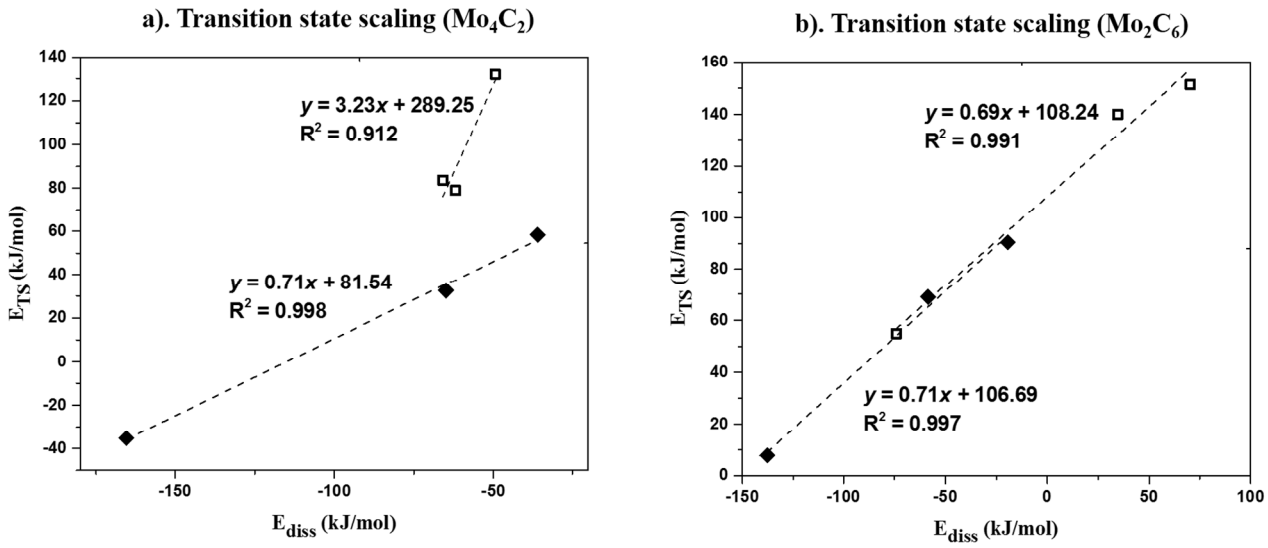

Figure 5. Linear scaling relationships between the energy of the transition states (E_{TS}) and corresponding dissociated chemisorption energy (E_{diss}) of the first (□) and second (◆) methane dehydrogenation steps on the (a) Mo_4C_2 and (b) Mo_2C_6 clusters.

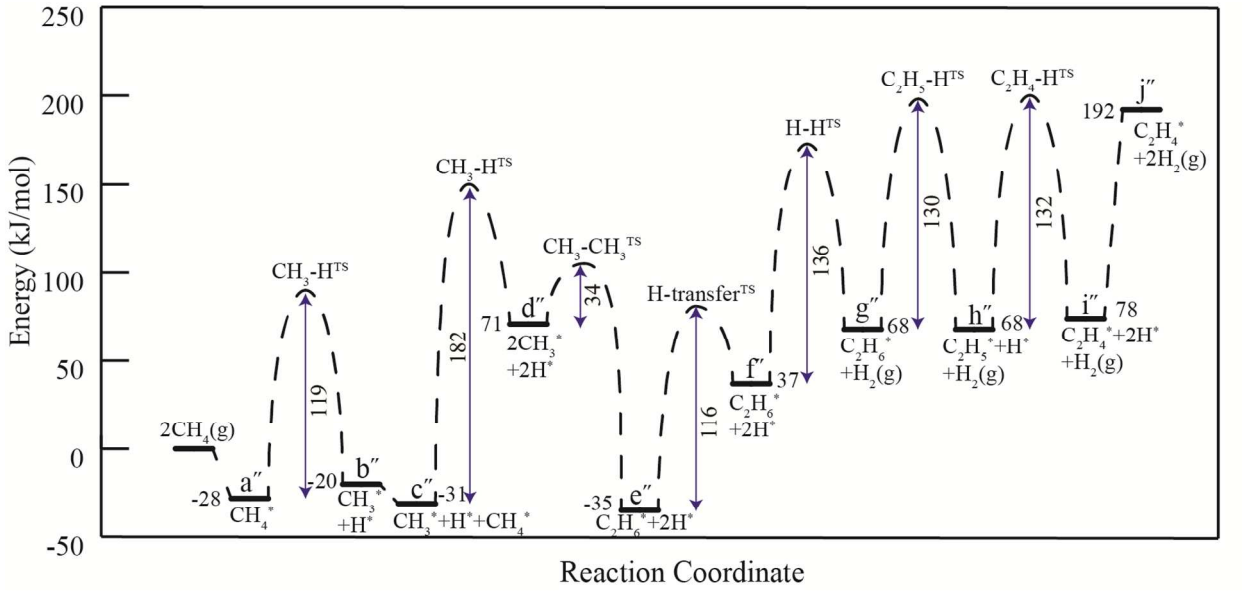

Figure 6. Reaction diagram for methane dehydrogenation and C-C coupling reaction to form ethylene on Mo_2C_6 cluster.

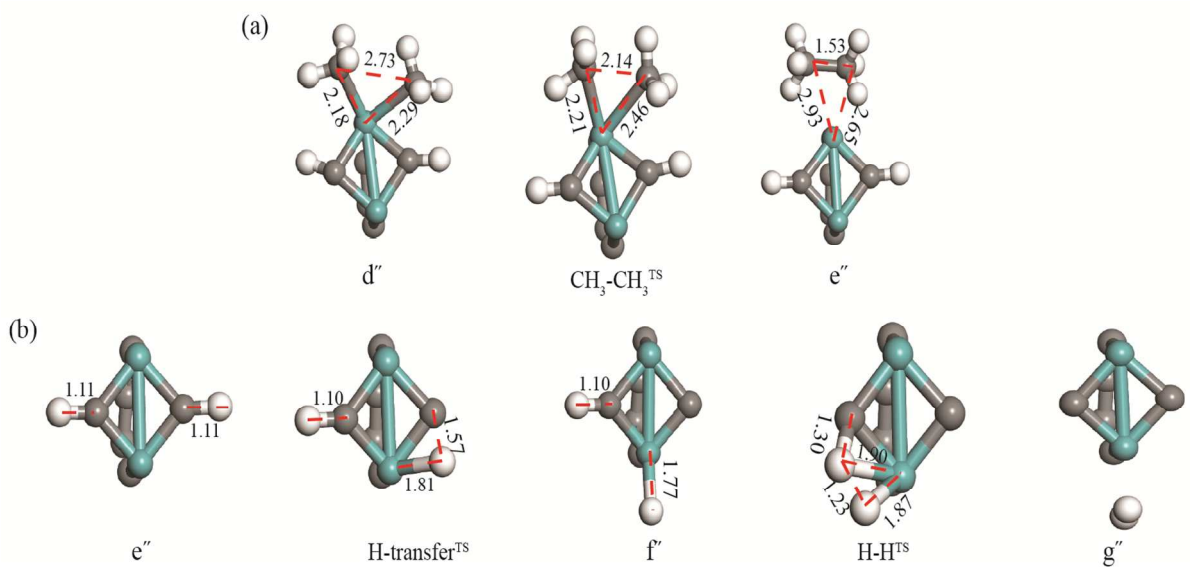

Figure 7. Geometry of the reactant, transition and product states for (a) coupling the two CH_3 species and (b) H_2 formation steps over the Mo_2C_6 cluster. (bond lengths in Å)

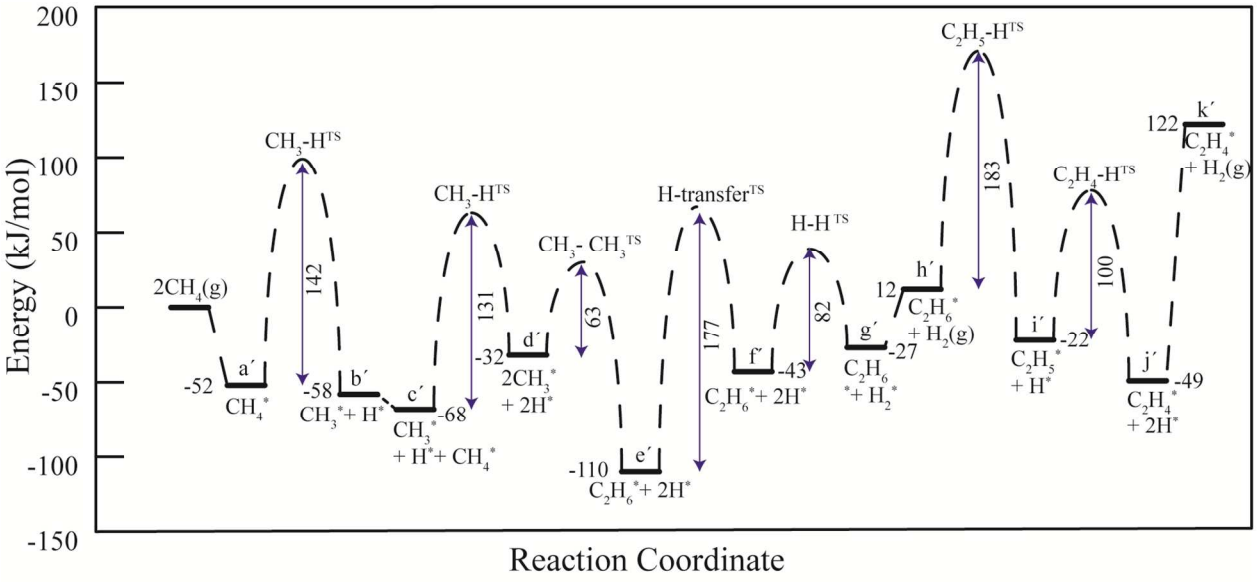

Figure 8. Reaction diagram for methane dehydrogenation and C-C coupling reaction to form ethylene on Mo_4C_2 cluster with +1 charge.

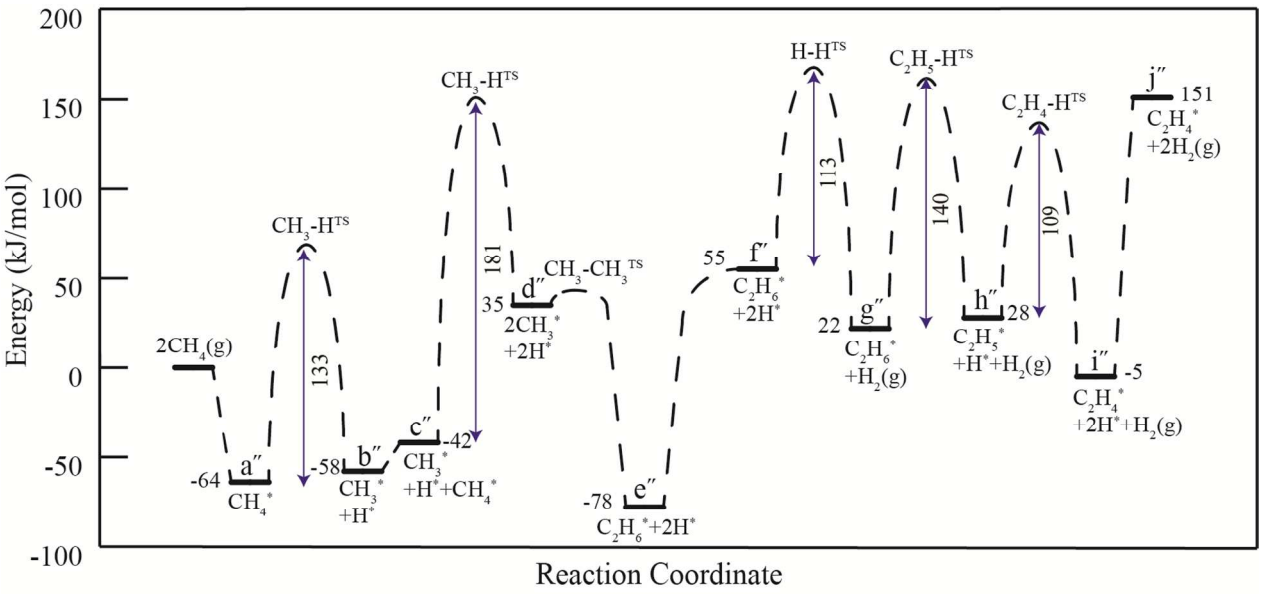

Figure 9. Reaction diagram for methane dehydrogenation and C-C coupling reaction to form ethylene on Mo_2C_6 cluster with +1 charge.

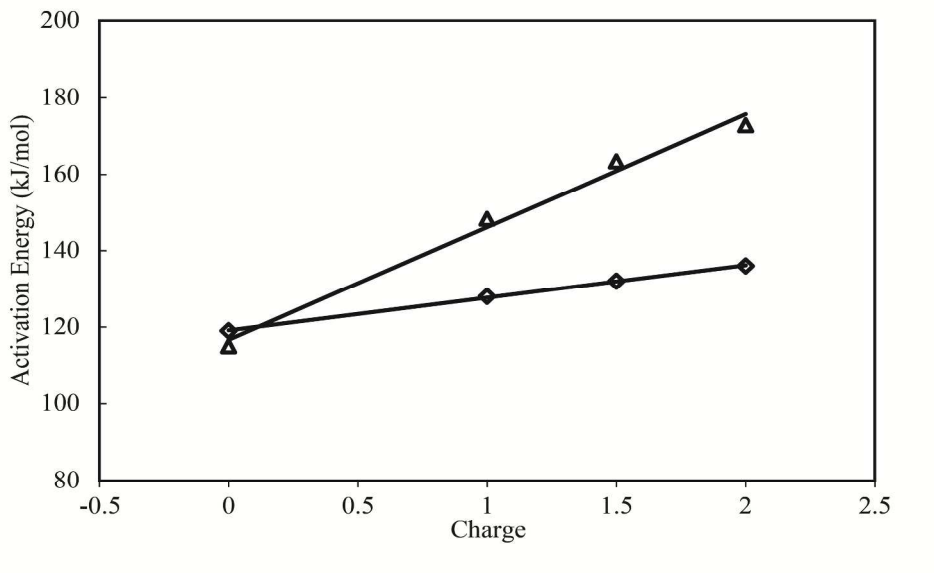

Figure 10. Effect of cluster residual charge on the first methane dehydrogenation activation barriers over Mo_4C_2 (triangle) and Mo_2C_6 clusters (diamond).

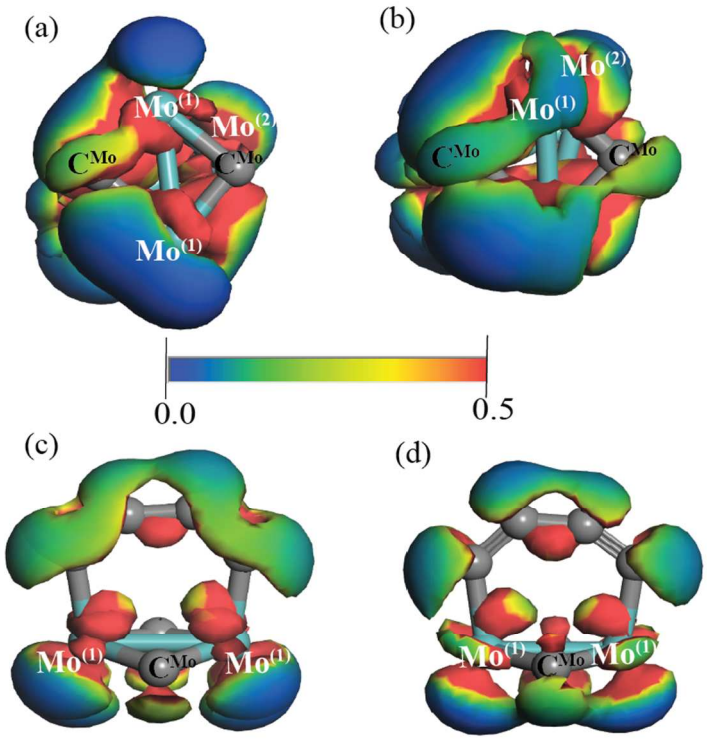

Figure 11. Electron density profile for; (a) neutral and (b) +1 charge Mo_4C_2 clusters; (c) neutral and (d) +1 charge Mo_2C_6 clusters